

Laser Powder Bed Fusion of Stainless Steel 316L using a flexible dual fiber laser array

T. Lantzsch*, T. Westphalen*, C. Tenbrock*, M. Traub*, and C. L. Haefner*

*Fraunhofer Institute for Laser Technology ILT, Steinachstrasse 15, 52074 Aachen, Germany

Abstract

In recent years, Laser Powder Bed Fusion (LPBF) has become an industrially established manufacturing technique. State-of-the-art LPBF machines feature a combination of fiber lasers and galvanometer scanners due to their high dynamic and excellent focusability. To increase the productivity of LPBF machines the number of laser scanner systems (LSS) is multiplied, which causes an almost linear increase of machine costs. In this study a flexible optical system which allows the combination of two fiber lasers with a single galvanometer scanner is developed and integrated into a LPBF lab machine to scale the productivity within one scan field. The resulting machine is characterized and used for the manufacturing of test specimen out of stainless steel AISI 316L. The manufactured specimens are analyzed in terms of melt pool formation via high-speed videography as well as resulting part density and build-up rate. The obtained results are compared with state-of-the-art LPBF-machines.

Introduction

Laser Powder Bed Fusion (LPBF) is an additive manufacturing (AM) technique capable of producing complex parts from metal powder. Thin powder layers with a typical thickness of $D_s = 20 - 100 \mu\text{m}$ are locally melted by a focused laser beam with a beam diameter between $d_s = 50 - 100 \mu\text{m}$. Due to the layer-wise manufacturing principle, LPBF is almost unlimited in terms of part complexity (i.e. inner cavities, overhangs) and is hence used in multiple industries such as aerospace, automotive and medical industry for the production of high-performance components in small to medium batch sizes. (1)

Nevertheless, LPBF still exhibits deficiencies with regard to productivity and process robustness (2). The simultaneous development of new LPBF machine concepts and processes thus holds the potential to overcome those deficiencies. A possible approach for the scaling of the LPBF productivity and robustness is the processing with multi-laser arrays.

Consequently, an optical system for the combination of two single mode fiber lasers with one galvanometer scanner is developed and integrated into a LPBF lab machine. This experimental setup is used for dual-laser LPBF experiments using stainless steel 316L. The laser powder interaction is analyzed via lateral high-speed videography for the determination of suitable processing strategies. In the following the experimental results are transferred to cubic specimens and compared with a single laser reference for LPBF process validation.

State of the Art

State of the art approaches for the scaling of LPBF productivity include the parallelization using multiple laser scanner systems (multi-laser LPBF) and the use of high laser powers in combination with larger focus beam diameters (high-power LPBF) (3, 4). For high-power LPBF the part is subdivided into a skin and a core area. While the skin is processed using a single-mode fiber laser with a maximum power of $P_{L,max} = 400 \text{ W}$ and a beam diameter of approximately $d_s = 90 \mu\text{m}$, the core is processed with a top-hat intensity profile and a beam diameter in the range of $d_s = 500 - 1000 \mu\text{m}$. In order to maximize productivity, a layer thickness which is typically 2-3 times larger is used for the core compared to the skin area (3).

In contrast multi-laser LPBF aims to reduce the build time by splitting the exposure area in every layer manufactured between multiple independent laser scanner systems (LSS). In principle this allows to increase the LPBF productivity by distribution of the exposure time between the LSS with a theoretical time reduction of $t_{exp, multi} = t_{exp, single} / n_{LSS}$, where $t_{exp, single}$ is the exposure time for a single laser LPBF system and n_{LSS} is the number of laser scanner systems (5). However, this productivity increase is practically limited by the part geometry and distribution within the machine's build envelope and further restrictions regarding processing strategies due to the interaction of the individual laser beams with the process by-products formed during LPBF processing (6). Hence, the full productivity potential of multi-laser LPBF machines can hardly be realized.

An alternative approach for increasing of LPBF productivity as reported in (5, 7, 8) is the utilization of multi-laser arrays for LPBF. In contrast to multi-laser LPBF approaches, the individual laser beams of multi-laser arrays cannot be positioned independently but follow a fixed geometrical relationship between each other. In (5, 8) multiple diode lasers are combined with fixed optics and mounted onto a gantry positioning system, while (7) uses fiber lasers as laser beam sources. However, compared to laser beam positioning via galvanometer scanners these approaches allow less dynamic laser beam movement across the powder bed. In (9, 10) two approaches based on galvanometer scanners are presented. Both approaches use diffractive optical elements (DOE) to split a single-mode incident laser beam into a plurality of partial laser beams with a fixed geometrical relation to one another. The generated multi-laser array is subsequently focused and moved across the powder bed using a galvanometer scanner. Due to the characteristics of the DOE the individual laser beams cannot be switched on and off individually. Furthermore, the beam splitting using a DOE results in power losses and hence reduces the system efficiency (10).

Approach and experimental setup

To allow LPBF processing via a flexible dual fiber laser array a suitable optical system that allows combination of two single mode fiber lasers with a single galvanometer scanner and a corresponding control system needs to be developed and characterized. The main consideration for the development of the dual laser optical system within this study is the compatibility with existing LPBF machines. A rendering of the final mechanical design as well as an overview of the final LPBF machine setup is depicted in Figure 1.

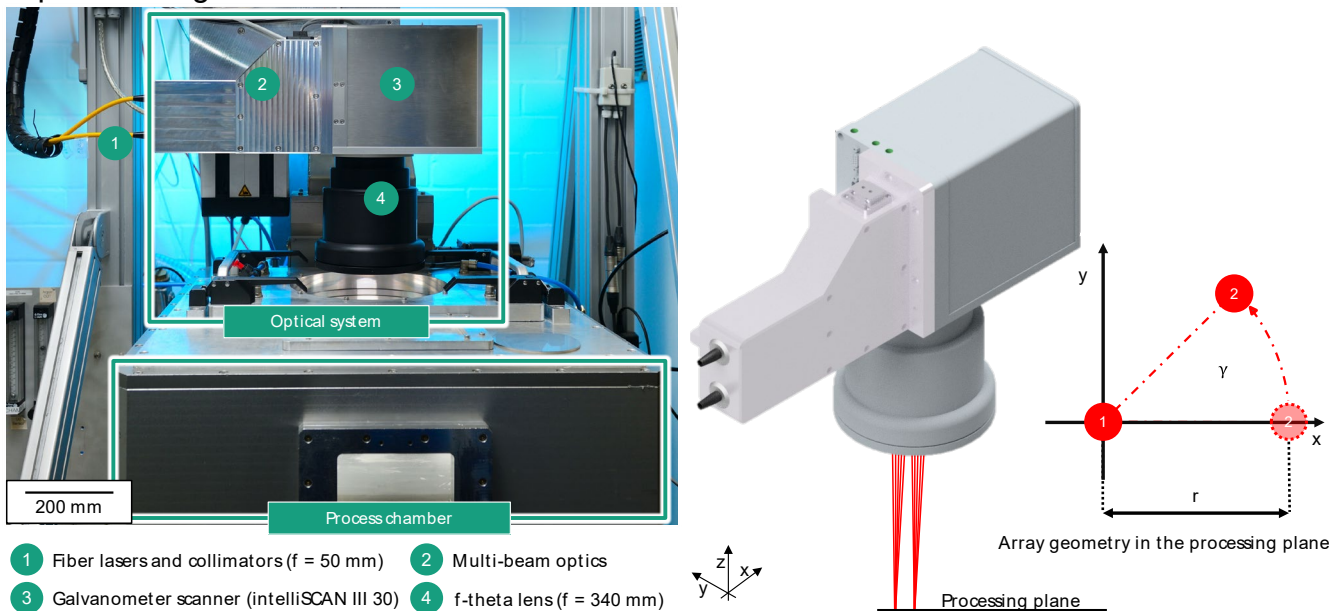


Figure 1: Machine setup for LPBF using a flexible dual fiber laser array (left) and corresponding dual laser optical system (right).

The developed dual laser optical system utilized the collimated incident laser beams of two single mode fiber lasers (IPG-YLR-400-WC, IPG Photonics Inc.). Moreover, the system is combined with a galvanometer scanner (intelliSCAN III 30, Scanlab GmbH) and an f-Theta lens ($f = 340 \text{ mm}$, $\lambda = 1030 - 1080 \text{ nm}$, Scanlab GmbH) for laser beam positioning and focusing. The dual laser optical system allows the flexible adjustment of the array geometry in a polar coordinate system by alteration of the position of the second laser spot relative to the first laser spot (c.f. Figure 1, right). The scanning motion required for the LPBF process is carried out by the galvanometer scanner while keeping a fixed array geometry. The entire optical system including galvanometer scanner and f-Theta lens is mounted onto a motorized z-axis to allow precise adjustment of the focal plane of the optical system and the processing plane of the LPBF machine. The machine setup is characterized regarding laser power characteristic and laser beam caustic for both utilized fiber lasers using a laser power meter (PRIMES cube, PRIMES GmbH) and laser beam profiler (Focus Beam Profiler FBP-F1K, CINOGY Technologies GmbH), respectively. The results of the laser characteristic and laser beam caustic measurements are summarized in Figure 2.

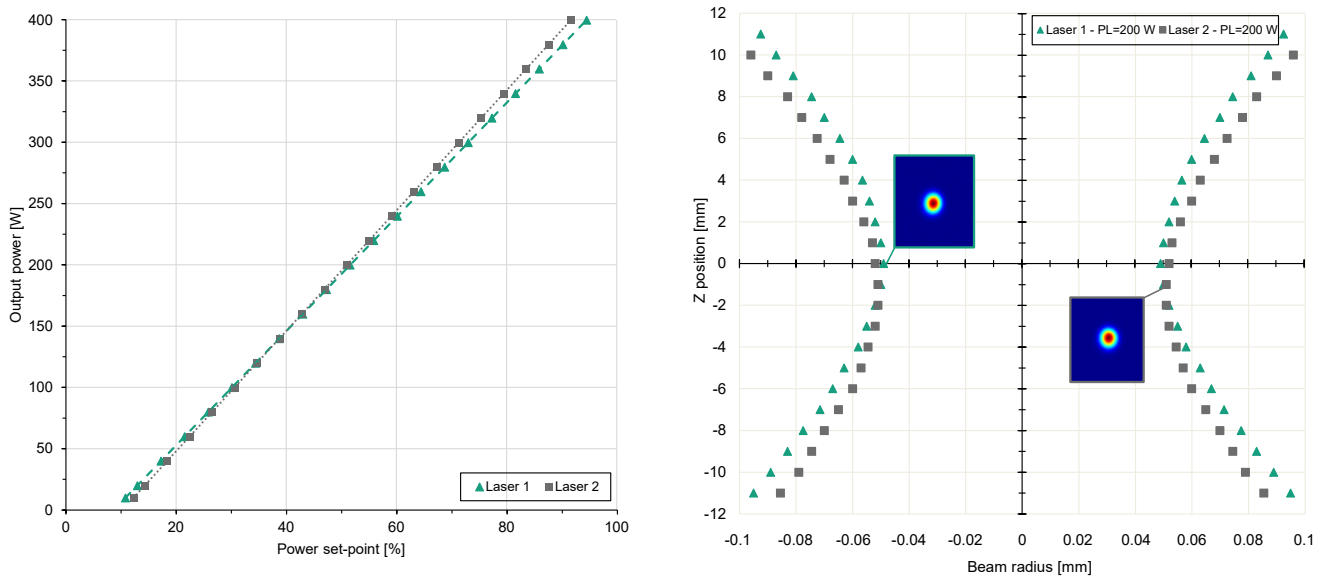


Figure 2: Laser power characteristic (left) and laser beam caustics (right) for utilized dual laser optical system.

The laser power characteristics for both lasers indicate a linear increase of laser power with increasing power setting. The slight difference in the respective slopes of the laser power characteristics is attributed to different calibration settings of the fiber lasers and can be compensated within the LPBF machine's control software. The laser beam caustic measurement indicates a Gaussian intensity distribution with a focus diameter of $d_s = 100 \mu\text{m}$ and a Rayleigh length of $z_R = 7 \text{ mm}$ for both laser beams. A focus position offset of approximately $\Delta z_0 = 0.5 \text{ mm}$ between laser 1 and 2 is detected. However, this offset yields a small beam diameter variation of $\Delta d_s = 4 \mu\text{m}$ and is hence negligible for the experimental investigations within this study. A summary of the used LPBF machine setup, the used components and the corresponding optical properties is exhibited in Table 1.

Table 1: Summary of utilized LPBF machine setup

LPBF machine setup	
Build area	Circular build platform Build platform diameter: 170 mm Max. build height: 200 mm
Laser beam source	2 x IPG YLR-400-WC (IPG Photonics Inc.) Water cooled single mode fiber laser with fixed collimator ($f = 50 \text{ mm}$) Max. output power: 400 W (cw) Wavelength: 1080 nm
Optical system	Dual laser opticals system intelliSCAN III 30 (Scanlab GmbH)

	f-Theta lens $f = 340$ mm (Scanlab GmbH) Focus beam diameter: $100\ \mu\text{m}$
Shielding gas	Argon O_2 -content < 100 ppm during LPBF processing
Powder deposition	Top-loader with soft recoater (silicon lip)
Modifications	Process chamber cover for high-speed videography Laser window for laser and illumination wavelength ($\lambda = 810$ and 1080 nm)

Methodology

All experiments within this study are conducted using AISI 316L stainless steel powder (m4p 316L, powder fraction $15 - 45\ \mu\text{m}$, m4p material solutions GmbH) Due to the additional degrees of freedom (i.e. laser power ration, array geometry), the LPBF process development for the flexible dual fiber laser array is characterized by a large number of possible parameter combinations. Therefore, the geometry of the dual fiber laser array is limited to spot distances r perpendicular to the scanning direction. A layer-to-layer rotation of the dual fiber laser array by 90° is realized via the machine control software. Furthermore, the laser power, scan speed and layer thickness are based on a single laser reference and kept constant at $P_L = 275$ W, $v_s = 1000$ mm/s and $D_s = 50\ \mu\text{m}$, respectively. The laser spot distance r and the hatch distance Δy_s are varied accordingly to allow manufacturing of simple cubic specimens ($10 \times 10 \times 10\ \text{mm}^3$) with a target relative density of $\rho_{\text{rel}} \geq 99.5\%$. The study is subdivided into first experimental series working with a laser spot distance which equals the laser focus diameter at $r = d_s = 100\ \mu\text{m}$ and a second experimental series working with a laser spot distance larger than the laser focus diameter ($r > d_s$). A schematic representation of the LPBF process development approach within this study is shown in Figure 3.

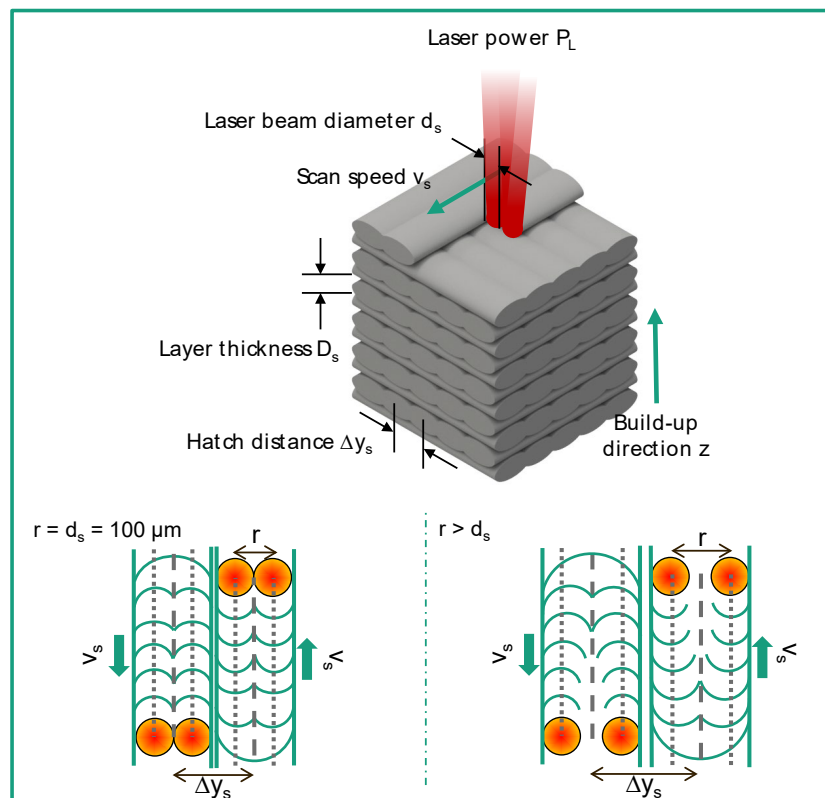


Figure 3: Process development approach for the manufacturing of volumetric specimens using LPBF with flexible dual fiber laser array.

A summary of the corresponding material data and reference process parameters is given in Table 2.

Table 2: Overview of powder material characteristics and LPBF processing parameters.

Material and LPBF process parameters	
Powder material	AISI 316L Powder supplier: m4p material solutions GmbH
Particle size distribution	Spherical, 15 – 45 μm
Laser power P_L	275 W
Scan speed v_s	1000 mm/s
Layer thickness D_s	50 μm
Scanning strategy	Bidirectional 90° hatch rotation between layers Feed direction against inert gas flow

In addition to the process development via simple cubic specimens, high-speed videography is employed to identify laser spot distances r that yield stable melt pool behavior. For this purpose, a lateral high-speed videography system is added to the machine setup. For the recording of high-speed videos of the LPBF process, the processing plane is illuminated by a collimated cw diode laser emitting at 808 nm. The used high-speed camera (Photron FASTCAM NOVA S16, Photron Inc.) is paired with a $f = 200$ mm fixed focal length camera objective (Nikon AF 200 mm 1:4 D, Nikon Corp.), a bandpass filter for the illumination wavelength (FB810-10, $\lambda_{\text{trans}} = 800 - 820$ nm, Thorlabs Inc.) as well as a bellow and observes the processing plane via a 45° mirror. A sandblasted copper plate is mounted onto the powder recoater and serves as a reflector to ensure diffuse illumination of the image region. An overview of the high-speed videography system is depicted in Figure 4.

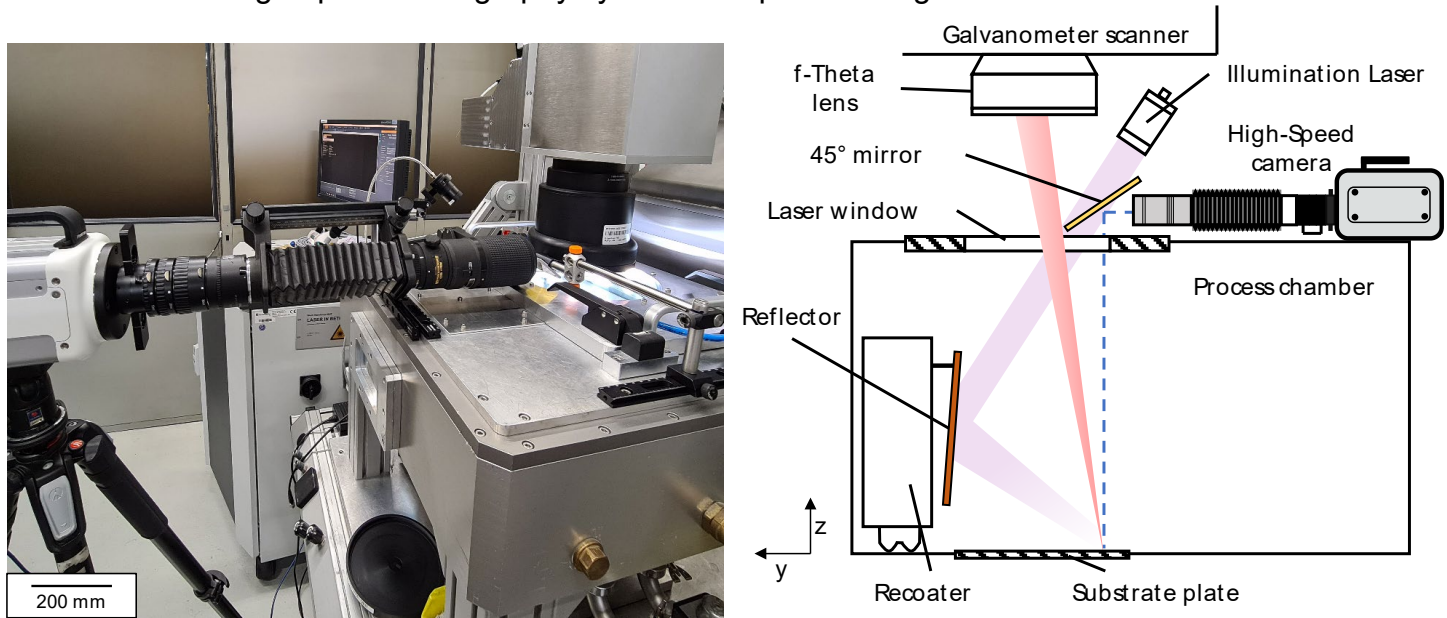


Figure 4: Setup for lateral high-speed videography of the LPBF process.

The resulting high-speed videos of the LPBF process are analyzed with regard to the melt pool dimensions of the individual melt pool generated by the dual fiber laser array and their respective interactions using the Photron Fastcam Viewer software (PFV4, Photron Inc.).

Results

High-speed images of the LPBF process with the flexible dual fiber laser array are analyzed regarding melt pool geometry. Additionally, the melt pool geometry and morphology of the top surface are determined based on pictures of etched cross section of the manufactured specimens (V2A etching agent, 60s) captured via optical microscopy (200x magnification, Keyence VHX-600, Keyence Corp.). The high-speed images and corresponding etched cross section for the LPBF process with a laser spot distance of $r = 100 \mu\text{m}$ and $r = 190 \mu\text{m}$ are depicted in Figure 5. The melt pool dimensions in the high-

speed images and the melt pool geometry in the cross-section images are highlighted by red lines, respectively.

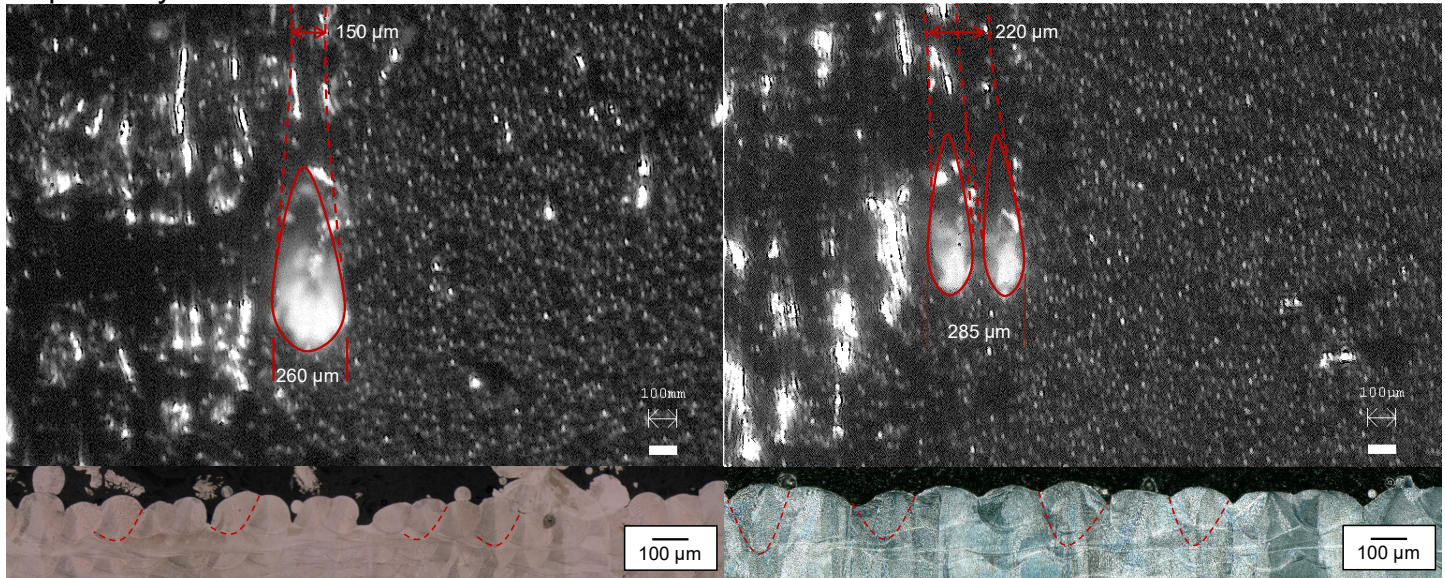


Figure 5: High-speed images of the of the LPBF process using a laser spot distance of $r = 100 \mu\text{m}$ (left) and $r = 190 \mu\text{m}$ (right). The corresponding melt pool geometries determined from etched cross sections of the manufactured specimens are depicted below.

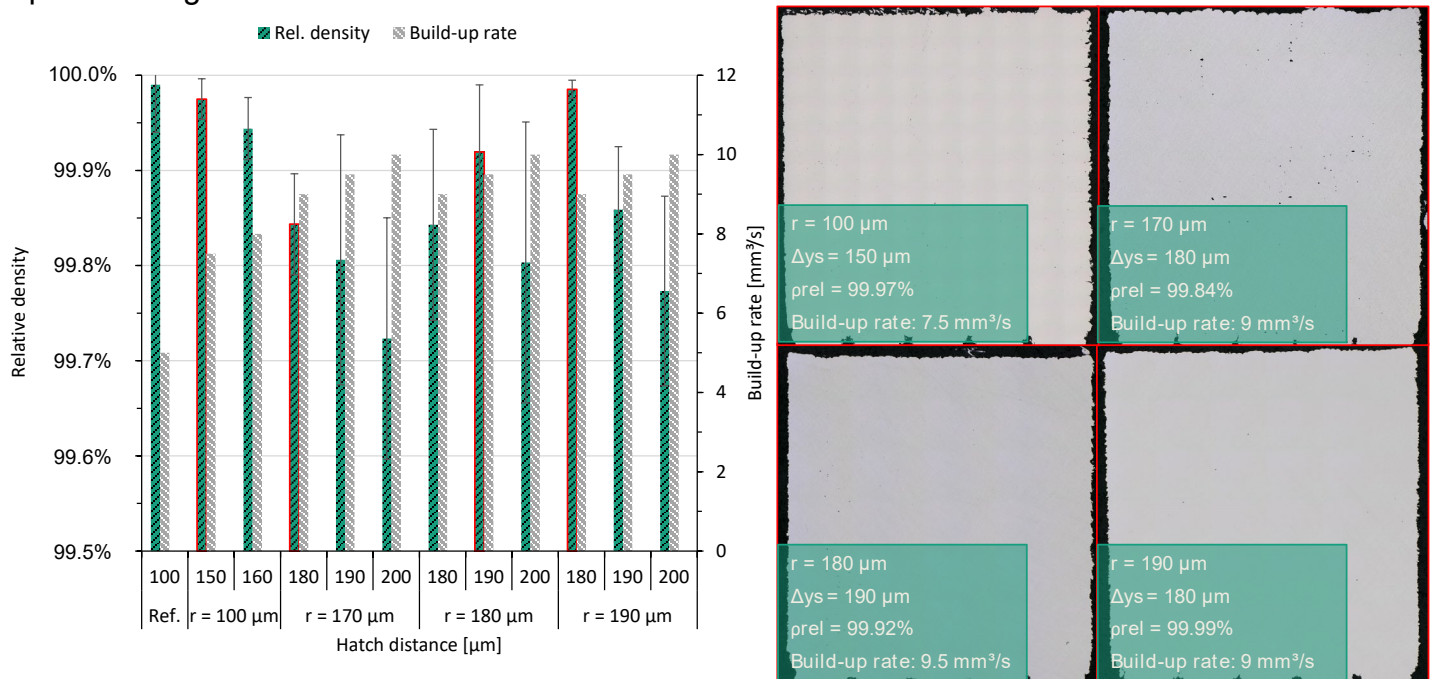
For a laser spot distance that equals the laser beam diameter ($r = d_s = 100 \mu\text{m}$, c.f. Figure 5 ,left) a strong interaction between the neighboring melt pools is observed. The laser spots of the array form two individual melt pools that exhibit a combined width of $w_{\text{mp,array}} = 260 \mu\text{m}$ in the region of the melt pool front. Subsequently, the individual melt pools unite and contract during solidification, resulting in a combined melt pool with of $w_{\text{mp,array}} = 150 \mu\text{m}$ after solidification. The observations from the high-speed images show good agreement with the melt pool geometry measured from the cross-section images, indicating a melt pool width of $w_{\text{mp}} = 150 \mu\text{m}$ and a melt pool depth of $t_{\text{mp}} = 154 \mu\text{m}$, respectively. Furthermore, an uneven surface morphology can be observed in the cross-section images. The strong interaction between the individual melt pool of the dual fiber laser array and the resulting melt pool union and contraction can be explained by a melt pool coalescence effect as investigated by (11). This effect results from the complex melt pool dynamics subsequently leading to the union of the melt pools in proximity to each other.

In contrast, the melt pool behavior changes with increased laser spot distance as indicated for $r = 190 \mu\text{m}$ (c.f. Figure 5, right). As for the smaller laser spot distance two individual melt pools, exhibiting a combined width of $w_{\text{mp,array}} = 285 \mu\text{m}$, are formed. However, these melt pools do not unite but stay separated until solidification yielding a combined melt pool width of $w_{\text{mp,array}} = 220 \mu\text{m}$. Furthermore, a movement of the melt pools towards the already solidified material can be observed. The melt pool width and depth measured from the etched cross-sections are found to be $w_{\text{mp}} = 130 \mu\text{m}$ and $t_{\text{mp}} = 100 \mu\text{m}$, respectively. These values show good agreement with the values determined for the single laser reference LPBF process with $w_{\text{mp}} = 125 \mu\text{m}$ and $t_{\text{mp}} = 108 \mu\text{m}$. The melt pool coalescence effect cannot be observed for laser spot distances of $r > 170 \mu\text{m}$, which agrees with the results obtained by Zhang et. al. (11).

The finding from the high-speed videography experiments are transferred to the LPBF manufacturing of cubic specimens with $10 \times 10 \times 10 \text{ mm}^3$. The relative density ρ_{rel} of the specimens is measured for three specimens per parameter combination via panoramic cross-section images at a 100x magnification using a Keyence VHX-6000 optical microscope (Keyence Corp.) followed by color thresholding. The laser spot distance r of the dual fiber laser array as well as the hatch distance Δy_s during LPBF processing are varied. The results are compared to the single laser reference LPBF process in terms of relative density ρ_{rel} and theoretical build-up rate \dot{V}_{th} . The theoretical build-up rate is calculated based on the scan speed v_s , hatch distance Δy_s and layer thickness D_s according to the following equation (1):

$$\dot{V}_{th} = v_s \times \Delta y_s \times D_s$$

The results of the relative density and build-up rate evaluation as well as the cross-sections for the parameter combination, that yield the maximum relative density for each laser spot distance r , are depicted in Figure 6.



For all investigated laser spot distances parameter combinations that yield a relative density of $\rho_{rel} \geq 99.5\%$ can be identified. Especially for larger laser spot distance of $r \geq 170 \mu\text{m}$ a larger scattering of relative density values with increasing hatch distance Δy_s is observed. The parameter combination, that yield the maximum densities for every laser spot distance r are highlighted in red. The corresponding cross-section images are exhibited on the right side in Figure 6. Except from $r = 170 \mu\text{m}$, parameter combination that yield a relative density of $\rho_{rel} \geq 99.9\%$ can be identified. For $r = 170 \mu\text{m}$ the cross-section indicates an uneven and wavy top surface structure. This behavior might be attributed to the transition from a strong coalescence effect between the individual melt pools towards a processing regime without melt pool coalescence as observed from the high-speed videos. Compared to the single laser reference process an increase of theoretical build-up rate by 90% from $V_{th} = 5 \text{ mm}^3/\text{s}$ to $V_{th} = 9.5 \text{ mm}^3/\text{s}$ can be achieved for a laser spot distance of $r = 180 \mu\text{m}$ and a hatch distance of $\Delta y_s = 190 \mu\text{m}$.

Summary and Outlook

In conclusion an optical system which allows flexible positioning of two single mode fiber lasers with a single galvanometer scanner was developed, integrated, and validated for the LPBF processing of stainless steel AISI 316L. Both laser beam sources of the optical system exhibit a linear laser power characteristic with a maximum output power of $P_{L,max} = 400 \text{ W}$ and a Gaussian intensity distribution with a focus beam diameter of $d_s = 100 \mu\text{m}$ for both laser beam sources. The analysis of the formation and interaction of the individual melt pools generated by the dual fiber laser array via lateral high-speed videography indicate a strong melt pool interaction for laser spot distances of $r \leq 170 \mu\text{m}$. In contrast laser spot distances of $r > 170 \mu\text{m}$ yield little to no interaction between the neighboring melt pools of the dual fiber laser array. Manufacturing experiments with varying laser spot distance r and hatch distance Δy_s while maintaining the laser power P_L , scan speed v_s and layer thickness D_s from a single laser reference are conducted. The investigated dual fiber laser array approach yields relative densities

of $\rho_{rel} \geq 99.9\%$ and theoretical build-up rates of up to $\dot{V}_{th} = 9.5 \text{ mm}^3/\text{s}$. This corresponds to a productivity increase of approximately 90% compared to the single laser reference process. Thus, the technological feasibility of the dual fiber laser array approach for the LPBF manufacturing of dense specimens at increased productivities is demonstrated within this study.

Nevertheless, the investigated approach still requires further investigation to prove its AM capabilities. As mentioned above the study at hand was solely centered around the development and validation of the dual fiber laser approach through evaluation of the relative part density. However, in order to prove application-ready manufacturing performance further research on part properties such as surface quality, mechanical properties and microstructure needs to be carried out. Additionally, the developed dual fiber laser optical system was only used to a fraction of its capabilities. This study exclusively addresses the dual fiber laser array working at a lateral laser spot distance r perpendicular to the scanning direction to increase the hatch distance Δy_s during LPBF processing. Further processing strategies such as a lateral spot distance r parallel to the scanning direction or dynamic oscillation of the second laser beam, as depicted in Figure 7, could leverage additional potentials for LPBF processing such as local pre- and post-heating or advanced control of melt pool behavior (12–14).

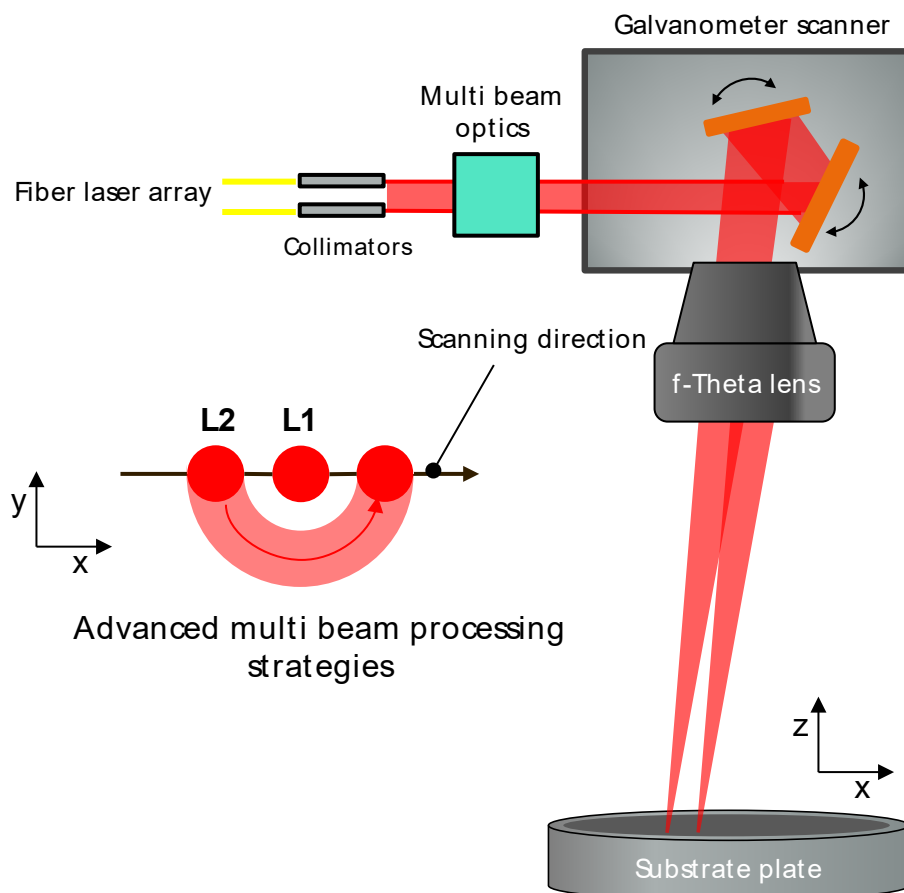


Figure 7: Utilization of flexible dual fiber laser array for advanced LPBF processing strategies.

These advanced LPBF processing strategies thus bear the potential to increase the processable material range (i.e. hard-to-weld/crack-prone materials) and process robustness (i.e. formation of process by-products, part distortion). Therefore, further research on the use of the developed flexible dual laser fiber array for advanced LPBF processing strategies will be conducted in the future.

Acknowledgements

The results presented within this article were generated as part of the Fraunhofer lighthouse project “futureAM – Next Generation Additive Manufacturing”.

Literature

- [1] MEINERS, Wilhelm. *Direktes selektives Laser Sintern einkomponentiger metallischer Werkstoffe*. Dissertation. Als Manuskript gedruckt, 1999. Berichte aus der Lasertechnik. 3-8265-6571-1.
- [2] SCHLEIFENBAUM, H., W. MEINERS, K. WISSENBACH, and C. HINKE. Individualized production by means of high power Selective Laser Melting [online]. *CIRP Journal of Manufacturing Science and Technology*. 2010, **2**(3), 161-169 [viewed 14 February 2019]. Available from: 10.1016/j.cirpj.2010.03.005.
- [3] SCHLEIFENBAUM, Johannes Henrich. *Verfahren und Maschine zur individualisierten Produktion mit High Power Selective Laser Melting*. Zugl.: Aachen, Techn. Hochsch., Diss., 2011. Aachen: Shaker, 2012. Berichte aus der Lasertechnik. 978-3-8440-0689-6.
- [4] BREMEN, Sebastian Wilhelm. *Korrelation der High Power SLM-Prozessführung mit der Produktivität, Effizienz und den Materialeigenschaften für den Werkstoff Inconel 718. Paralelltitel auf dem Promotionstitelblatt: Correlation of high power SLM process with productivity efficiency and material properties for inconel 718*. 1. Auflage. Aachen: Apprimus Verlag, 2017. Edition Wissenschaft Apprimus. 978-3-86359-516-6.
- [5] EIBL, Florian. *Laser powder bed fusion of stainless steel with high power multi-diode-laser-array*. Dissertation. 1. Auflage. Edition Wissenschaft Apprimus. 978-3-86359-587-6.
- [6] TENBROCK, Christian, Tobias KELLIGER, Niklas PRAETZSCH, Marcel RONGE, Lucas JAUER, and Johannes Henrich SCHLEIFENBAUM. Effect of laser-plume interaction on part quality in multi-scanner Laser Powder Bed Fusion [online]. *Additive Manufacturing*. 2021, **38**, 101810. Available from: 10.1016/j.addma.2020.101810.
- [7] KARP, Jason H., Victor OSTROVERKHOV, David BOGDAN, Michael GRAHAM, Brian MCCARTHY, and William CARTER. Area melting with multi-laser arrays to increase build rate for metal powder bed fusion additive manufacturing. In: Henry Helvajian, Bo Gu, and Hongqiang Chen, eds. *Laser 3D Manufacturing VI*: SPIE, 2 Feb. 2019 - 7 Feb. 2019, p. 8.
- [8] ZAVALA-ARREDONDO, Miguel, Nicholas BOONE, Jon WILLMOTT, David T.D. CHILDS, Pavlo IVANOV, Kristian M. GROOM, and Kamran MUMTAZ. Laser diode area melting for high speed additive manufacturing of metallic components [online]. *Materials & Design*. 2017, **117**, 305-315. Available from: 10.1016/j.matdes.2016.12.095.
- [9] SLODCZYK, Marcel, Alexander ILIN, Thomas KIEDROWSKI, and Vasily PLOSHIKHIN. Influence of multi-spot exposure of powder bed on melt pool stability in selective laser melting. In: Henry Helvajian, Bo Gu, and Hongqiang Chen, eds. *Laser 3D Manufacturing VI*: SPIE, 2 Feb. 2019 - 7 Feb. 2019, p. 7.
- [10] TSAI, Chun-Yu, Chung-Wei CHENG, An-Chen LEE, and Mi-Ching TSAI. Synchronized multi-spot scanning strategies for the laser powder bed fusion process [online]. *Additive Manufacturing*. 2019, **27**, 1-7. Available from: 10.1016/j.addma.2019.02.009.
- [11] ZHANG, Wenxuan, Wenyuan HOU, Luc DEIKE, and Craig B. ARNOLD. Using a dual-laser system to create periodic coalescence in laser powder bed fusion [online]. *Acta Materialia*. 2020, **201**, 14-22. Available from: 10.1016/j.actamat.2020.09.071.
- [12] MATTHIAS, Simon, Marc LUCAS, Seetharam SIVAM, and Bhavesh BHUT. Using wobble based laser scanning techniques in additive manufacturing applications. *Lasers in Manufacturing Conference*. 2019, **2019**, 1-13.
- [13] HEELING, Thorsten, and Konrad WEGENER. The effect of multi-beam strategies on selective laser melting of stainless steel 316L [online]. *Additive Manufacturing*. 2018, **22**, 334-342. Available from: 10.1016/j.addma.2018.05.026.

[14] CAO, Liu. Numerical Investigation on Molten Pool Dynamics During Multi-laser Array Powder Bed Fusion Process [online]. *Metallurgical and Materials Transactions A*. 2021, **52**(1), 211-227. Available from: 10.1007/s11661-020-06076-6.